Attitude Determination System for a Nadir-Pointing Satellite

W.F. Havens* and H. Ohtakay†
Jet Propulsion Laboratory, Pasadena, Calif.

An attitude determination system for a nadir-pointing satellite with a high inclination orbit is investigated. The major engineering difficulty of such a system lies in estimating the nadir direction due primarily to large uncertainties of Earth atmospheric conditions caused by seasonal and diurnal variations over a wide range of latitude. Presented in this paper are investigation results of an attitude determination system approach which automatically adapts itself to those variations and augments the end-to-end attitude determination accuracy of science-sensor boresights through in-flight calibration. The engineering approaches discussed in this paper will be applied to the SEASAT-A mission.

I. Introduction

HIGHLY accurate satellite attitude determination is required to allow proper interpretation of science data. In addressing this problem for the SEASAT-A mission, an Attitude Determination (AD) System was conceived to focus the issues affecting science instrument pointing accuracy determination. The SEASAT-A mission science payload and satellite have been discussed in detail in Refs. 1 and 2. That information which affects the AD system is summarized briefly here.

SEASAT-A provides a proof-of-concept mission whose objectives include demonstrating techniques for global monitoring of oceanographic phenomena and features, providing oceanographic data for both application and scientific users, and determining key features of an operational ocean dynamics monitoring system. Scheduled for launch in mid-1978 into a near-polar, 800-km orbit, the SEASAT-A mission is planned to last one year, beginning with several weeks allotted to final adjustment of the operational orbit, and testing and calibration activities. The basic measurement objectives of the ocean experiments will be met by a payload consisting of five instruments – three active radiators and two passive receivers. The radiators include the radar altimeter (ALT), the SEASAT-A scatterometer system (SASS), and the synthetic aperture radar (SAR). The receivers are the visual and infrared radiometer (VIRR) and the scanning multichannel microwave radiometer (SMMR).

SEASAT-A is a nadir-oriented satellite, so the determination of the nadir direction is an important part of the AD process. Coarse nadir direction is established by the Orbiter Attitude Control System (OACS) for the purpose of satellite attitude control, while the same data telemetered to the ground will be used for AD.

The AD system is that set of satellite hardware and ground software which provides information about the line-of-sight attitude of each science instrument. The inputs to the system are the sun and horizon references and the satellite environment. The output is a set of time-ordered estimates and uncertainties of the line-of-sight of each science instrument. System hardware consists of attitude sensors – two infrared horizon scanners and two sun aspect sensors – and their electronics, telemetry system, science instruments, and the satellite structure on which the hardware is mounted. The ground software consists of the definitive attitude determination (DAD) software that provides a time history of the attitude of the satellite reference axes, and that portion of the footprint determination (FPD) software which relates the satellite reference axes to the lines-of-sight of the science instruments.

Several challenging engineering problems have been encountered in the implementation of the AD system. The use of sun sensors instead of star scanners or trackers for yaw AD has necessitated the interpolation rather than measurement of yaw attitude during solar eclipses – about 25% of mission time. Sun sensor field-of-view (FOV) limitations extend the mission time without direct yaw attitude measurements by another 25%. Newly developed horizon scanners have required extensive modeling and Earth atmospheric radiance studies. The sensitivity of science data quality to AD accuracy for this science payload has required much study in order to assure that science requirements complement AD capabilities.

II. AD System Design Considerations

A. Satellite Hardware

The sun aspect sensors, each consisting of two 2-axis sun sensor heads, digitally measure sun aspect angles with a resolution of 1/256 deg. The sun aspect sensors are not a part of the OACS, but are used only for yaw AD.

The infrared (IR) horizon scanner is an attitude sensor designed to detect continuously the direction of the local vertical throughout the normal orbital flight of the satellite. Since SEASAT-A is in a polar orbit, one horizon scanner often is looking at the lit portion of the planet while the other views the dark part. Differences in these two limbs complicate the nadir determination. The horizon scanner consists of a scanning IR temperature-sensing device and electronics. The IR temperature-sensing device, i.e., the bolometer, generates signals proportional to IR energy in the spectrum passband of the scanner optical system. The scanner conically rotates with a half-cone angle of 45 deg around a vector tilted 26 deg from the pitch axis in the pitch-yaw plane. The 2×2 deg square FOV optics attached to the bolometer have been designed to have a narrow spectrum passband, as shown in Fig. 1, whose maximum response characteristic[3] is located about 15 μm from the spectrum line. During the design of such a spectrum passband, the Earth's atmospheric luminosity was taken into consideration. The Earth's atmospheric luminosity was computed as a function of latitude, seasonal and diurnal variations, and altitude. The primary contributor to the incoming energy is the 15μm radiance from carbon dioxide, augmented with radiance from ozone and water vapor. As the FOV rotates at the nominal rate of 900 rpm (with the allowed variation of $\pm$300 rpm), the bolometers output high-level signals whenever the horizon scanners "look at" the Earth's

Presented as Paper 77-1037 at the AIAA 1977 Guidance and Control Conference, Hollywood, Fla., Aug. 8-10, 1977; submitted Sept. 19, 1977; revision received Feb. 16, 1978.

Index categories: Spacecraft Navigation, Guidance, and Flight-Path Control; Sensor Systems; Atmospheric and Space Sciences.

*Technical Group Supervisor, Guidance and Control Section.
†Member of Technical Staff, Guidance and Control Section.

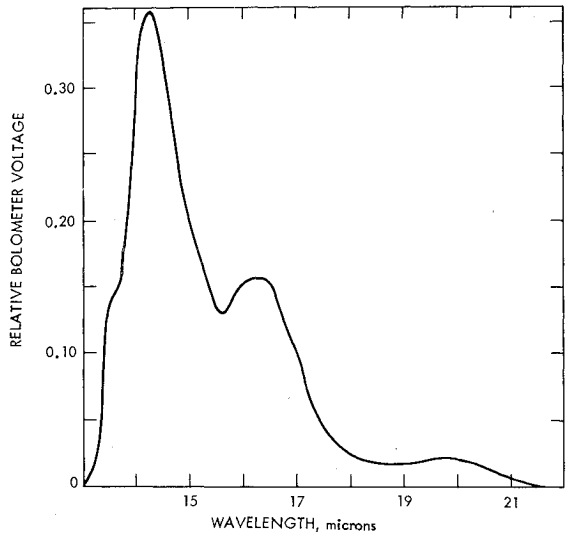

Fig. 1 Scanner optical filter spectrum passband.

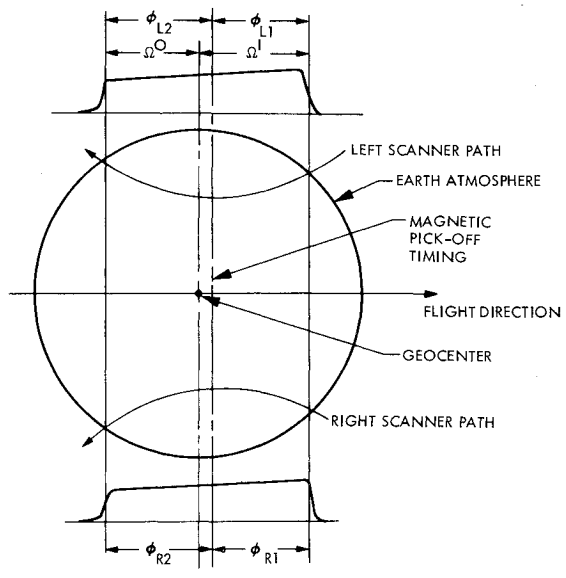

Fig. 2 Scanner signals and timing.

atmospheric regions and zero level signals when the scanner boresights are directed toward the "cold sky." The abrupt change in sensed IR emissions as the bolometer transitions from the cold sky to Earth's atmosphere and back results in the sensor output being a series of pulses. Figure 2 illustrates the scan geometry with respect to the Earth, pulse widths of the Earth, and signal timing.

The variable thresholding method of the Earth's horizon pulse signal sensing, intended to self-adjust for the Earth radiance variations, is achieved by the following. The Earth pulse widths from the reference timing are determined by slicing the pulse with variable thresholding levels. These variable thresholding levels are automatically determined by the onboard electronics, such that the scan angle η_c at the horizon triggering instant satisfies the following relationship. First, an average pulse height is determined through

$$g = \frac{1}{|\eta_1 - \eta_2|} \int_{\eta_1}^{\eta_2} g(\xi)\,d\xi \tag{1}$$

where g is a pulse signal of the Earth's atmosphere at the pulse thresholding circuit. Then, the atmospheric horizon boundaries are determined so that the relationship

$$g(\eta_c) - k_v g = 0 \tag{2}$$

is satisfied during the rise and the fall of an Earth pulse, corresponding to the scan into and out from the Earth's atmosphere, where k_v is a constant representing the percentage threshold level desired. The Earth pulse thresholding and the duty cycle pulse-generating circuitry is called a locator.

The salient aspects of the variable thresholding technique employed in the locator include accounting for the diurnal and seasonal variations of the Earth's atmosphere since g is determined by the observed radiance level of g, and compensating for the Earth pulse shape asymmetry, which is caused by bolometer thermal lag and preamplifier frequency characteristics.

Earth pulse widths, $\emptyset_{ij}$, $i=(L, R)$, and $j=(1, 2)$ (Fig. 2), determine the satellite attitude pitch and roll orientations, denoted by p_s and r_s, respectively, through

$$\begin{bmatrix} p_s k_p \\ \\ \\ r_s k_r \end{bmatrix} = \begin{bmatrix} -1 & 1 & -1 & 1 \\ & & & \\ & & & \\ -1 & -1 & 1 & 1 \end{bmatrix} \begin{bmatrix} \phi_{L1} \\ \phi_{L2} \\ \phi_{R1} \\ \phi_{R2} \end{bmatrix} \tag{3}$$

where k_r and k_p are constants. The sensor pitch and roll angle pairs are computed through Eqs. (1-3) by the attitude computer and are provided to OACS for satellite control. These measurements are also telemetered back to the ground station after appropriate signal conditioning, sampling, and quantization.

The science instruments also constitute a part of the AD system, in that their alignments are needed to determine the instrument boresight attitude, and these instruments can be used for in-flight calibration of the AD sensors to augment the AD system performance accuracy. The ground calibration alignment values of the science instruments will be used for translating the satellite axes AD into the science instrument boresight AD until an in-flight calibration is performed. Discussions about the in-flight calibration will be made in the forthcoming subsections.

B. Ground Software

The primary functions of the AD ground software are to enhance the accuracy of the telemetered AD sensor data and to compute the science instrument boresight attitudes to assist science instrument data interpretation. The other important functions of the ground AD software system include yaw attitude determination for sun data gap periods, attitude telemetry data conditioning and validating, and AD output data quality assurance.

AD accuracy enhancement by the ground software is achieved in two ways: 1) the compensation of known systematic errors in the AD sensor measurements through better modeling of the Earth's physical parameters and precise satellite definitive orbit determination data; and 2) the interpretation and application of in-flight calibration data.

The systematic correction to the telemetered attitude sensor data is performed[4] to first-order acruracy of the error perturbation. The main reason for this lies in the limitation of the accuracy of the available data base for such a correction process, i.e., a higher order correction does not improve the total AD accuracy.

The following includes discussion of corrections to systematic errors due to the Earth's oblateness (Δp_{obl} and Δr_{obl}), the atmospheric radiation variation (Δp_{rad} and Δr_{rad}), and the satellite altitude variation (Δp_{alt} and Δr_{alt}).

The oblateness perturbation terms (Δr_{obl} and Δp_{obl}) are modeled through the geometric relationship of the satellite altitude and the Earth's atmospheric boundaries triggering the horizon scanners for a particular scan. Figures 3 and 4 show the geometric relationship among satellite attitude angles,

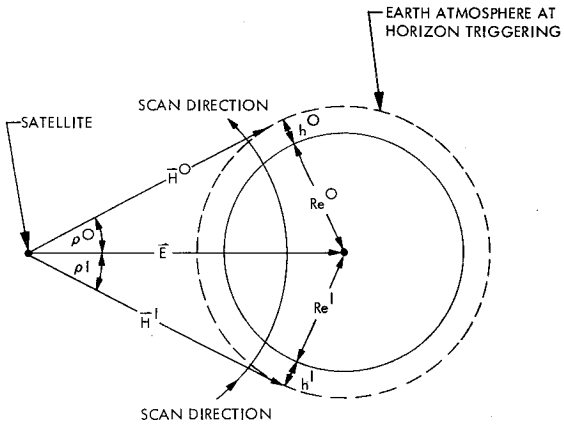

Fig. 3 Earth satellite geometry – a side view.

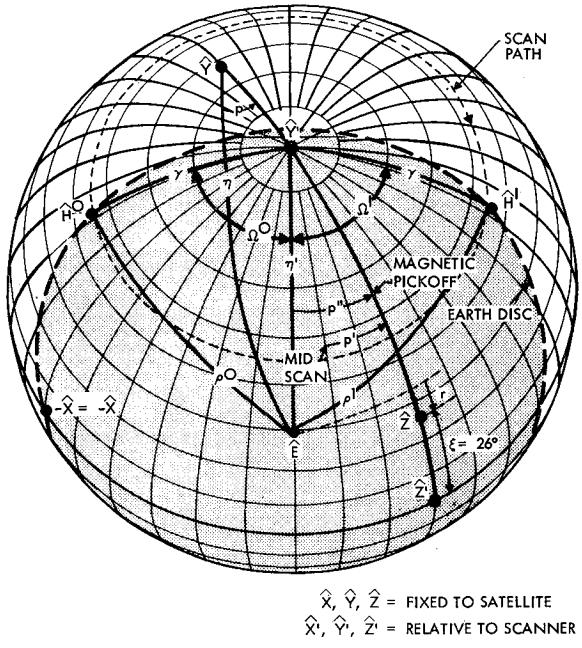

Fig. 4 Scanner and satellite attitude geometry as viewed from the scanner.

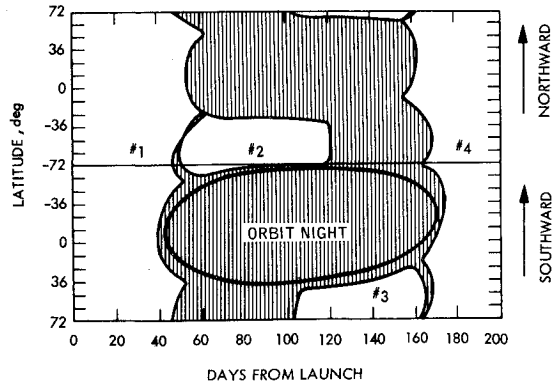

Fig. 5 Sun data availability schedule.

horizon scanner measurement angles, and the Earth. For satellite roll attitude r, there exists a relationship

$$\sin r = (\cos\eta_L' - \cos\eta_R')/2\cos\xi \tag{4}$$

where η_i' is the satellite nadir angle of scanner boresight direction measured by the right and left scanners, $i=(R,L)$ and ξ is the angle between scanner rotation axis and a plane perpendicular to satellite nadir axis (nominally 26 deg).

Since the right-hand side of Eq. (4) is a function of $R_i^{I,0}$, $h_i^{I,0}$ and E with $i=(R, L)$ (where $R_i^{I,0}$ and $h_i^{I,0}$ represent the Earth radii and the tangent heights for horizon crossing and E the satellite-Earth distance as shown in Fig. 5), the needed correction to roll telemetry value for oblateness effect is given by

$$\Delta r_{\text{obl}} = \frac{1}{2\cos r}\sum_{i=(R,L)}\left(\frac{\partial f^I}{\partial R_i^I}\Delta R_i^I + \frac{\partial f^0}{\partial R_i^0}\Delta R_i^0\right) \tag{5}$$

where the functions f^I and f^0 represent the right-hand side of Eq. (4) corresponding to scans into (superscript I) and out of (superscript 0) the Earth's atmosphere, respectively. The partial derivatives in this equation, as well as in those which follow, are to be evaluated with a set of nominal values of independent parameters involved. The correction term to compensate radiance variation effects may be treated essentially in the same way, since $R_i^{I,0}$ and $h_i^{I,0}$ appear only as a linear sum form in functions f^I and f^0. Hence,

$$\Delta r_{\text{rad}} = \frac{1}{2\cos r}\sum_{i=(R,L)}\left(\frac{\partial f^I}{\partial h_i^I}\Delta h_i^I + \frac{\partial f^0}{\partial h_i^0}\Delta h_i^0\right) \tag{6}$$

The correction terms to compensate the satellite altitude variation effects is readily given, through the preceding discussions, as

$$\Delta r_{\text{alt}} = \frac{1}{2\cos r}\sum_{i=(R,L)}\left(\frac{\partial f^I}{\partial E_i}\Delta E_i + \frac{\partial f^0}{\partial E_i}\Delta E_i\right) \tag{7}$$

An interesting aspect of this correction term is that the output error magnitude from each scanner due to altitude variations is the same, and such errors cancel to zero when they are substituted into Eq. (3), because both scanners will operate practically at the same altitude. Therefore, the correction given by Eq. (7) needs to be applied only when either one of the scanners is not operating due either to hardware malfunction or to the sun being in the FOV.

Accuracy of the telemetered pitch angle can be improved by compensating for the known systematic error due to oblateness and Earth atmospheric radiance effects. For the scanner geometry,

$$\tan p = \tan p'' \cos\xi \tag{8}$$

where p is the satellite pitch angle and p'' is the true scanner pitch angle.

Expressing the measured scanner pitch angle p' in terms of p'' and the Earth pulse duty cycles Ω^0 and Ω^I (Fig. 4) as

$$p' = p'' + (\Omega^0 - \Omega^I)/2 \tag{9}$$

where Ω^I is the in-scan to geocenter scan pulse width, Ω^0 is the geocenter to out-scan pulse width, the correction term δp_i is given by

$$\delta p_i = -\frac{\Omega_i^0 - \Omega_i^I}{2}\cos\xi \tag{10}$$

with $i=(R, L)$.

Hence, oblateness effect correction Δp_{obl} is now given by

$$\Delta p_{\text{obl}} = \frac{1}{2}\sum_{i=(R,L)}\delta p_i \tag{11}$$

to the first-order accuracy of the correction term. The radiance variation effect can be corrected essentially in the same way as explained for that of roll.

C. Yaw Interpolation

Figure 5 shows predicted sun data availability as a function of the position of the satellite in its orbit and the number of days from launch. The numbers in the figure indicate the sun sensor head identifiers. The satellite flight position is given in terms of the Earth latitude of the subsatellite point and direction (i.e., northbound or southbound) of flight. For an orbit of a given day, the sun availability can be ascertained by simply drawing a vertical line spanning the figure. Only when the line crosses a clear region does a sun sensor head see the sun. In the shaded regions, the sun is either occulted or is outside the FOV of all sun sensor heads. From this figure, it is observed that for about 50% of mission time no sun sensor sees the sun, implying no direct attitude measurement.

Definitive AD processing will take place three to four days after engineering telemetry data playback from the satellite. This lag is sufficient to assure that sun measurement data immediately before and after any sun data gap are simultaneously available for use in the yaw determination process. This implies that the gap-filling process may be performed by means of a generalized interpolation method. An algorithm was developed[5] for this purpose, utilizing a hybrid technique of data smoothing, extrapolation by autocorrelation of yaw, a priori prediction, and indirect measurements.

D. In-flight Calibration

In-flight calibration can be used to improve AD accuracy by facilitating the compensation of structural and instrument misalignments impossible or very expensive to measure on the ground. Discussed here are two in-flight calibration approaches. One is the in-flight calibration of the horizon scanner alignments based upon sun sensor measurements. The other is the calibration of the attitude sensor and science instrument alignments based upon science instrument data. The former calibration is intended for AD accuracy augmentation at the satellite body reference axes. The latter is aimed at enhancement of the end-to-end science instrument boresight AD accuracy and verification of the flight performance of the science instruments.

The attitude sensors measure directions to the two independent references – the sun and the local vertical. This implies that, in general, four independent elements are measured. The AD process may be characterized as computation of three independent elements, i.e., roll, pitch, and yaw. The excess information is utilized to conduct the in-flight calibration of one of the attitude sensors based upon the other. The sun sensors, having better measurement accuracy, may be used as primary sensors to calibrate the horizon scanners which are inherently less accurate. The limiting accuracy of this calibration is the total measurement accuracy of the primary sensors with respect to the satellite alignment reference axes.

In-flight calibration of the attitude sensors based upon the science instrument data is also a viable approach. This type of in-flight calibration is intended to re-establish the end-to-end alignments from the attitude sensors to the science instruments and can be performed by comparing the science instrument measurement data against the ground truth data. In the case of SEASAT-A, the science instrument data base will be supplemented by data taken by the attitude sensors. The landmark observation performed by science instruments, e.g., SAR and VIRR, may be included in the in-flight calibration data base. Due to the extremely high measurement resolution of these science instruments, it is anticipated that performance accuracy to the level of theoretical limits of the science instrument resolution is feasible.

III. Performance Accuracy Assessment

Discussed here are the performance accuracy assessment at the system component level, particularly for those components and their interacting elements having significant impact upon the performance accuracy, the total AD system performance accuracy with respect to the accuracy requirements, and the science data sensitivity to the AD system performance accuracy.

A. Atmospheric Radiance Effects

The IR horizon scanner is sensitive to IR energy in the spectrum passband of the scanner optical system. The selection of the spectrum passband region of operation is one of the most important steps in the design of the horizon scanner. This selection was made based upon a tradeoff influenced by many factors, the most important of which are the properties of the horizon radiation, the sun's radiation, and the available knowledge of these elements during the satellite flight. Other factors taken into consideration include the satellite orbit parameters and the scan pattern of the IR scanner. In applications where high accuracy is the prime requirement, a spectrum region should be selected to minimize the angular instability of the horizon sensing.[6] The 15 μm CO_2 band satisfies such a requirement. Furthermore, the specific spectrum width with best stability encompassing this band has been shown[7] to extend from 14.0 to 16.3 μm, with the potential detected horizon stability better than 1 km. The spectrum passband of the horizon scanner optics for SEASAT-A (Fig. 1) exhibits basic agreement with the CO_2 passband requirement, except the prolonged extension of the passband characteristics in the longer wavelength region.

In order to assess the expected performance accuracy of the horizon scanner prior to launch of the satellite, an Earth atmospheric model has been developed. The atmospheric temperature, pressure, and density are modeled for the average values of April and July as a function of latitudes in the northern and southern hemispheres. The altitude regime includes from the ground level to 110 km. The original data base was derived from balloon and rocket observation measurements[7] and partially augmented by the selective chopper radiometer (SCR) data from NIMBUS IV. The deficiencies of this model are that 1) it is an average over time and space (longitude) which may not reflect the local variability of the atmosphere, although the SCR data proved that, except for stratospheric warmings, the monthly averaged atmosphere provides a reasonable representation; and 2) the original data base was mostly limited to that for the northern hemisphere.

Once the atmosphere is specified, an emitted radiation can be calculated. The total radiance sensed is the integral of all radiance molecules in the optical path. The contribution of each portion of an optical path is proportional to the temperature, emissivity $E(\lambda)$, and transmissivity $t(\lambda)$ of that portion through the atmosphere. The basic expression for radiance, denoted by $N(\lambda)$ normalized for the collecting aperture and the scanner FOV, is given by

$$N(\lambda) = \beta(\lambda)E(\lambda)t(\lambda)_{s=s_0} + \int_{s_0}^{s} \beta(\lambda)E(\lambda)t(\lambda)\,dS \qquad (12)$$

where $\beta(\lambda)$ is the blackbody radiation of incremental path dS, λ is the wavelength, and S is the optical path.

The received radiance is further modified by the scanner spectrum passband q (Fig. 1).

$$N = N(\lambda)q(\lambda) \qquad (13)$$

Figure 6 shows the relative magnitudes of the unfiltered clear atmospheric radiance, radiance through the SEASAT-A spectral passband characteristics, and the unfiltered spectrum radiance for an opaque cloud at the tropopause. The data base has been selected to be that for July at the equator, since such a data base would represent a highly wet region and hence would constitute a most severe condition to the horizon scanners. From this figure it can be seen that clouds have a

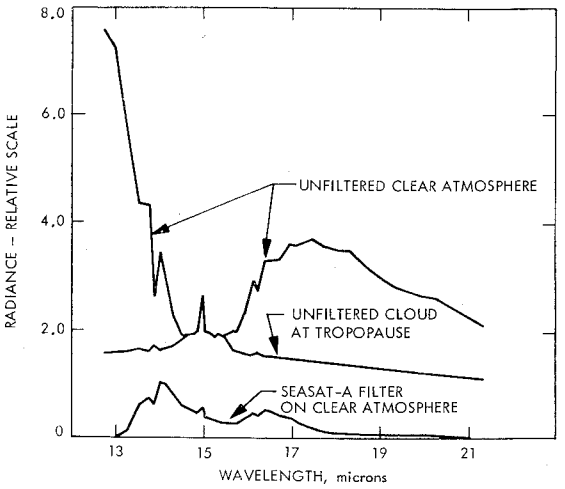

Fig. 6 Radiance spectrum comparison.

significant effect on the radiance profile and the scanner does show sensitivities to input energies in the region of $16 \sim 17 \mu m$.

Other important findings identified[8] during the Earth atmospheric modeling study include: a 200% increase in the ozone level in the Earth's atmosphere at all altitudes had a negligible effect on the radiance profile; variations of radiance profile due to the Earth's local surface conditions, i.e., ocean, land, or desert, for a same latitude and season were insignificant; and atmospheric water vapor variability was observed to be more significant with the SEASAT-A optical filter than a narrower filter whose transfer characteristic cut off around 16.5 μm.

In the wavelength region of $16 \sim 17$ μm, ozone and water radiance become significant and the horizon scanner shows significant response sensitivities in this region (Fig. 6), almost comparable to that around the 15 μm region. The radiance profile in the 15 μm CO_2 passband has been observed to exhibit deterministic[9,10] variations with time and latitude, as well as random variations. In order to enhance the pitch and roll sensor accuracy, a systematic compensation of the deterministic atmospheric radiance variation effects is planned. For this purpose, the atmospheric radiance profile data have been compiled for the spectrum passband of the SEASAT-A scanner optics and integrated over the monthly variation and over all longitudes for a given latitude. Such data have been prepared for the months of April and July in the northern and southern hemispheres in 10-deg increments of latitude. By assuming symmetry between the northern and southern hemispheres in opposite seasons, the April and July data are equivalent to four months of data in both hemispheres. The atmospheric radiance data base for the rest of the eight months has been interpolated from these equivalent four months of data.

The atmospheric radiance data, equivalently passed through the scanner optical system by filtering it with the optics spectrum passband, has been used to evaluate the performance accuracy of the scanner and its electronics. The objectives of such a study are to assess how well the variable thresholding technique described in the previous section is adjusting itself to variations of the atmospheric radiance; to evaluate quantitatively the unaccounted error boundaries of the pitch and roll AD and the limiting accuracy of the horizon scanner and its electronics; and to investigate the impact of the atmospheric radiance variability upon the pitch and roll AD accuracies.

The simulated scanner bolometer signal $S_{I(t)}$ was computed as a function of the scanner's spin rate W_0 as

$$S_I(t) = R(W_0 t) \tag{14}$$

This consideration made it possible to investigate the scanner performance variation as a function of the scanner

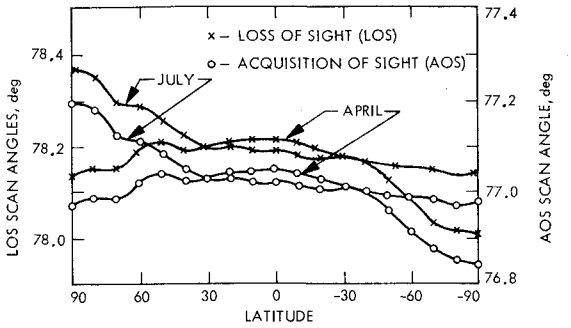

Fig. 7 Scan angle variations.

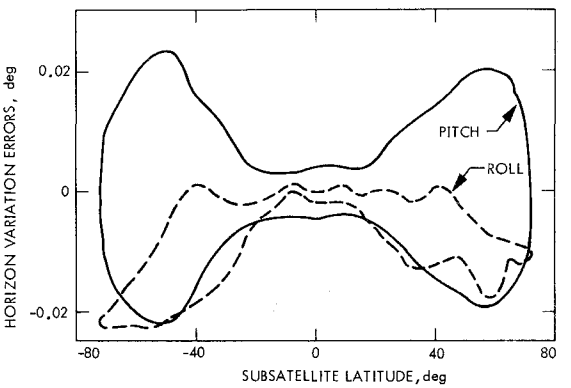

Fig. 8 Roll and pitch sensor errors due to atmospheric radiance variation in July.

spin rate. The scanner electronics transfer function $H(2\pi f)$ for the block of linear electronic circuitry, starting at the bolometer output terminal and ending at the thresholding circuit, i.e., the horizon locator, was analytically derived. The time domain expression $h(t)$ of $H(2\pi f)$ was first computed to form the output to the locator $g(t)$ through

$$g(t) = \int_{-\infty}^{t} S_I(t)\ h(t-t')\,dt' \tag{15}$$

The locator, in turn, simulates Eqs. (1-3), the output of which was then compared with the known satellite attitude motion.

Figure 7 illustrates the scan angle variations at the acquisition of sight (AOS) and loss of sight (LOS) thresholds for the months of April and July where the stratospheric effect is not included. AOS and LOS of the scanner angle η are separated by an almost constant angle, which is caused by the thermal lag of the bolometer and frequency characteristics of the scanner preamplifier electronics, including the pulse-

Table 1 Expected roll and pitch AD performance accuracy

Error sources	Roll (deg, 3σ)	Pitch (deg, 3σ)
Random horizon radiance variation	0.173	0.104
Noise in IR scanners	0.010	0.010
Scanwheel speed variations	0.002	0.029
Temperature variations of scanners	0.069	0.069
Locator stability	0.069	0.069
Attitude computer drift	0.055	0.055
Sun sensor accuracy	0.050	0.050
Launch shock (sun sensors)	0.010	0.010
Sun sensor alignment errors	0.003	0.003
Thermal distortion	0.073	0.073
In-flight calibration uncertainties	0.010	0.010
RSS Total	0.225	0.180

shaping circuit. It is interesting to note that in the equatorial region the AOS and LOS scanner angles are quite stable and, more importantly, the seasonal variation is small; in the polar regions, the seasonal variations of AOS and LOS scan angles are more significant.

Figure 8 depicts the unaccountable errors in the pitch and roll sensors for one complete orbit of the satellite. This type of error is caused mostly by the atmospheric variation effect and the uncompensated errors in the horizon locator with variable thresholding levels. As can be expected from Fig. 7, the error values are small in the equatorial region, while larger error magnitudes are observed toward the polar regions. It should be noted that these errors are nonstationary for satellite orbit position and seasonal changes, which implies that compensation of these errors by ground software is extremely difficult.

B. Roll and Pitch Attitude Determination

The anticipated performance accuracies of the roll and pitch AD are given in Table 1. In this table, the error entry due to atmospheric variation effect has been computed based upon Figs. 7 and 8, and multiplying a factor to account for the atmospheric radiance variations not included in the data base used in this study. Such additional error sources include diurnal atmospheric radiance variations, latitudinal variations, residual error in seasonal variations caused by data base construction by means of interpolation, and the stratospheric radiance effect, i.e., the cold-cloud effect. From Table 1 it is concluded that the major error source in determining the satellite nadir direction is the random variation of atmospheric horizon radiance largely contributed by cold-cloud variations in the stratosphere.

C. Yaw Attitude Determination

The yaw AD accuracy when sun data are available is given by a function of the sun data measurement accuracy with respect to the satellite alignment reference axes. Errors in the sun data measurement, denoted by Δs, are summarized in Table 2. The yaw AD error, denoted by Δy, is now given in terms of Δs by

$$\Delta y = \sqrt{2(1-\Delta x)} \tag{16}$$

where

$$\Delta x = (\cos\Delta s - \cos^2\lambda)/\sin^2\lambda$$

The worst-case yaw AD error, at the edge of the wide angle sun sensor FOV of 64 deg on a side, is computed through the preceding equation to be 0.231 deg (3σ).

Verification of the yaw AD algorithm outlined in Sec. II for the sun data gap periods was performed, based upon a set of simulated attitude motion data. These simulated data were generated for a nominally designed SEASAT-A with typical internal misalignments, various initial conditions, and typical external disturbance conditions. The sun-gap conditions, except the sun-eclipse condition, were artificially created during the performance verification study. This approach made it feasible to evaluate performance statistically for sufficiently large sample sizes.

Table 2 Sun sensor measurement performance accuracy

Error sources	Sun sensor error (deg, 3σ)
Transfer function error	0.061
Dynamic alignment shift	0.008
Mounting alignment uncertainty	0.003
Sensor mounting thermal distortion	0.046
Pitch and roll coupling into yaw	0.180
RSS total	0.231

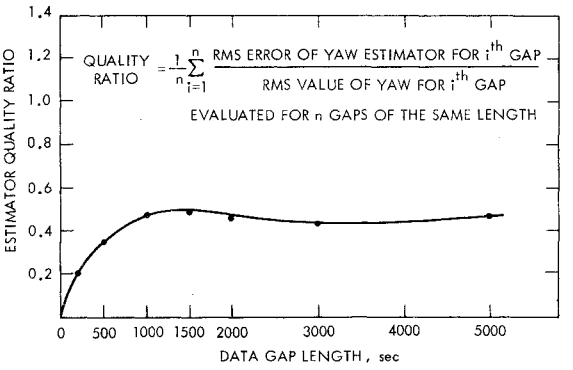

Fig. 9 Yaw interpolation algorithm performance accuracy.

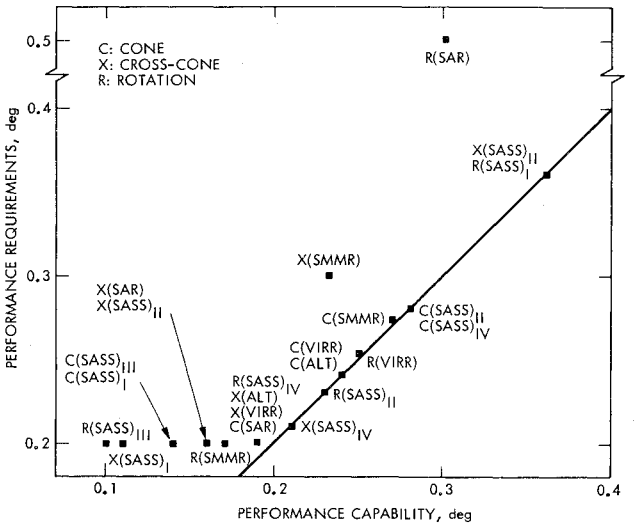

Fig. 10 Science instrument boresight AD requirements vs performance accuracy.

Figure 9 shows the predicted performance accuracy of the yaw interpolation algorithm in terms of the estimator quality ratio for a discrete set of gap lengths. For this figure, the performance accuracy is predicted to be 0.5 deg (3σ) for the longest gap of slightly longer than 5000 s, provided that: 1) the magnitude of yaw attitude motion of SEASAT-A does not exceed 0.8 deg, the yaw control accuracy; 2) true yaw attitude motion has dynamic characteristics similar to those of the simulated data; 3) indirect data measurement, i.e., the roll rate, is as significant an indicator of yaw in flight as it was in simulation; and 4) the error contribution caused by the roll rate calculation is sufficiently small.

D. AD Sensitivity Analysis

A sensitivity analysis would, in general, reveal deviation of a system's nominal performance caused by variations of performance characteristics of system components. The sensitivity analysis performed here is characterized as a quantitative assessment of the degree of degradation (or improvement) of science instrument data quality as a function of AD accuracy, particularly near the boundaries of such accuracy requirements. Figure 10 shows the relationship between the AD accuracy requirements and the AD system performance accuracy at individual science instrument boresights. In this figure, any data points appearing on the left-hand side of the broken line indicate that the required accuracies are being met. It is seen that SASS AD requirements are only marginally satisfied. For this reason, the discussion in the following material focuses on the sensitivity analysis of SASS.

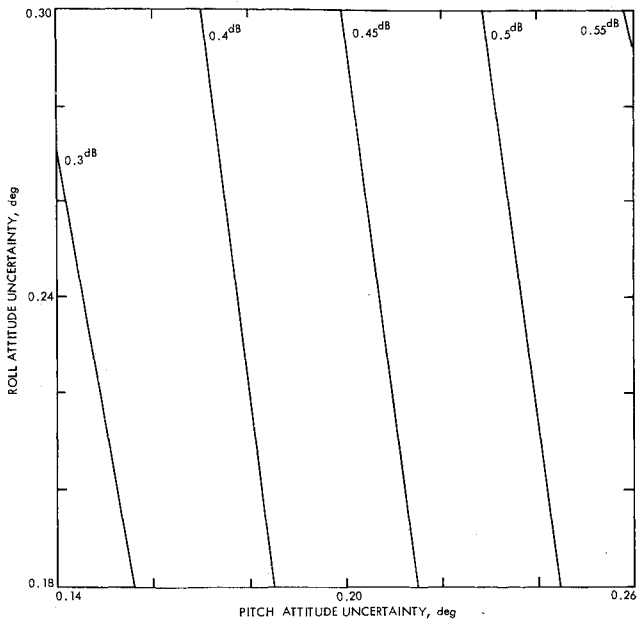

Fig. 11 SASS AD accuracy sensitivities: σ° variation plot for constant yaw accuracy.

Any sensitivity analysis requires a priori establishment of performance indices. Such indices are desired to have the same physical quantities, or at least represent the same physical concept, for all the science instruments involved. The mean cross section per unit area, denoted by σ° and called the backscattering coefficient, has been used for an index to represent the SASS data quality. Similar investigation for ALT is feasible by replacing σ° with the signal-to-noise ratio. The backscattering coefficient σ° can be expressed in terms of the determined attitude of roll (r), pitch (p), and yaw (y) together with SASS unique error parameters, ϵ_i, $i=(1,2,3,\ldots)$, as

$$\sigma^\circ = f(r,p,y,\ \epsilon_1,\epsilon_2,\epsilon_3,\ldots) \tag{17}$$

Hence, the variation $\Delta\sigma^\circ$ in σ° due to AD perturbations Δr, Δp, and Δy, is given by

$$\Delta\sigma^\circ = \delta f \Delta^T \tag{18}$$

where

$$\delta f = (\partial f/\partial r, \partial f/\partial p, \partial f/\partial y) \qquad \Delta = (\Delta r, \Delta p, \Delta y)$$

The partial derivatives comprising the components of δf are to be evaluated at the set of attitude angles of interest, i.e., the requirement values of the AD system accuracy. Equation (18) constitutes the SASS sensitivity coefficient with respect to the AD system performance accuracy. The variability of such a sensitivity coefficient is given by the second moment of Eq. (18) as

$$\sigma^2(\Delta\sigma^\circ) = E[\Delta\sigma^{\circ 2}] = \delta f E[\Delta^T \Delta]\delta f^T \tag{19}$$

where $E[\ ]$ is the expectation operator.

Figure 11 illustrates the dB error in σ° for the constant yaw AD accuracy of 0.23 deg (3σ) and at subsatellite latitude of 0 deg. Figure 12 delineates the dB error in σ° for constant roll and pitch AD accuracy of 0.23 and 0.18 deg (3σ), respectively, and at the same subsatellite latitude. Although elaborate discussions of these errors in terms of wind speed measurement accuracy is beyond the scope of the AD system performance accuracy evaluation, such dB errors in σ° have been confirmed to lie within the boundaries of the SASS mission requirements. Important conclusions derived from the sensitivity analysis are: 1) σ° is most sensitive to the pitch AD uncertainty and 2) the SASS data quality will follow gradual degradation if there were an increase in the AD uncertainties beyond the AD performance accuracy requirements.

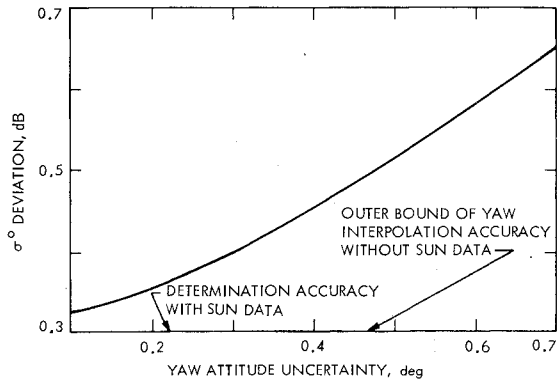

Fig. 12 SASS AD accuracy sensitivities: σ° variation for constant roll and pitch accuracies.

IV. Conclusion

The AD system performance for a nadir-pointing satellite with a high inclination orbit has been evaluated in the end-to-end sense, where emphasis was placed upon SEASAT-A application. It has been found that the largest error source for reconstructing the satellite attitude, particularly the nadir direction, lies in uncertainty of Earth horizon radiance variations. To understand better the effect of AD errors on science instrument data quality, a science instrument performance sensitivity analysis was completed. It has been confirmed that the most AD-accuracy-critical science instrument, i.e., SASS, showed only gradual degradation in performance in the vicinity of the anticipated AD performance capability boundaries.

Acknowledgment

This paper represents one phase of research carried out at the Jet Propulsion Laboratory, California Instutute of Technology, under NASA Contract NAS 7-100. The following people contributed to the work which is reported in this paper: E.M. Bracalente, R.Z. Fowler, R.J. Hendricks, G.M. Lerner, J. Lorell, G.F. Meyers, M.C. Phenneger, and A.J. Treder.

References

[1] Cutting, E., Born, G.H., Frautnick, J.C., McLaughlin, W.I., Neilson, R.A., and Thielen, J.A., "Mission Design for SEASAT-A, An Oceanographic Satellite," AIAA Paper 77-31, Los Angeles, Calif., Jan. 1977.

[2] Weiss, W., Rodden, J.J., Hendricks, R.J., and Beach, S.W., "SEASAT-A Attitude Control System," *Journal of Guidance and Control*, Vol. 1, Jan.-Feb. 1978, pp. 6-13.

[3] "Scanwheel Pitch and Roll Attitude Determination Accuracy in the SEASAT Configuration," Ithaco Inc., Rept., No. 91179, Aug. 1976.

[4] Phenneger, M.C., Meyers, G.F., et al., "SEASAT-A Attitude System Functional Specifications and Requirements," Computer Science Corporation, CSC/SD-77/6001, March 1977.

[5] Treder, A.J., "A Hybrid Technique for Spacecraft Attitude Interpolation with Arbitrary Attitude Data Gaps," *Modeling and Simulation*, Vol. 8, Proceedings of the 7th Annual Conference, Pittsburgh, pp. 209-217.

[6] Thomas, J.R., Wolfe, W.L., et al., "Spacecraft Earth Horizon Sensors," NASA SP-8033, Dec. 1969.

[7] Bates, J.C., et al., "The Synthesis of 15 Micron Horizon Radiance Profiles from Meteorological Data Inputs," NASA CR-724, April 1967.

[8] Keithley, P.L. and Uplinger, W.G., "Atmospheric Radiance Profiles for the Ithaco Horizon Sensor," EM No. B3.1-007, Lockheed Missile and Space Co., Inc., April 1977.

[9] McKee, T.B., Witman, R.I., and Davis, R.E., "Infrared Horizon Profiles for Summer Conditions from Project Scanner," NASA TN D-4741, Aug. 1968.

[10] Witman, R.I., McKee, T.B., and Davis, R.E., "Infrared Horizon Profiles for Winter Conditions from Project Scanner," NASA TN D-4905, Dec. 1968.